COMMUNICATIONS

# Interfacial Microstructure of Chromium Oxide Coatings**

By *Xiaolu Pang, Kewei Gao,* * *Huisheng Yang, Lijie Qiao, Yanbin Wang* and *A. A. Volinsky*

Chromium oxide coatings are chemically inert, have high mechanical strength, hardness and good optical characteristics; therefore, they have been widely used in many applications including corrosion protection,[1] wear resistance,[2] electronics,[3] and optics.[4]

$Cr_2O_3$ is well suited for wear resistance applications, as it is one of the hardest oxides with 29.5 GPa hardness.[5] Several deposition techniques have been tried for making these coatings. $Cr_2O_3$ coating hardness can vary substantially due to compositional and microstructural variations, depending on the deposition method. Hardness of a plasma-sprayed $Cr_2O_3$ coating, 50 μm thick was about 14.7 GPa, while a 200 nm thick RF-sputtered chromium oxide coating, stoichiometrically close to $Cr_2O_3$, exhibited 30 GPa hardness combined with good scratch resistance.[6] Even for the bulk $Cr_2O_3$, hardness values reported were from 9 GPa to 29.5 GPa.[5,7,8] Hones *et al.* investigated a correlation between the hardness and the sputtering deposition parameters,[2] i.e. oxygen partial pressure and substrate temperature, and found favorable deposition conditions with an oxygen partial pressure of about 15–20 % of the total sputtering gas pressure at substrate temperatures exceeding 500 K.

Good coating adhesion is required for wear and corrosion resistance applications. Premature failure can occur for many reasons including coating delamination, cracking and plastic deformation. In addition to this, thin ceramic PVD coatings usually have columnar grain structure with micro cracks, pinholes, transient grain boundaries and often high through-coating porosity, which all lead to accelerated pitting corrosion and failure at the coating/substrate interface, especially in hostile environments.[9–12] On the other hand, several studies showed that coating thickness plays an important role in enhancing both PVD-coated tool cutting performance and resistance to abrasive and erosive wear.[13]

Graded systems have been employed to obtain thicker coatings without losing performance in terms of coating adhesion and toughness.[14] It is likely that thicker coatings will improve corrosion resistance in aqueous environments by eliminating through-thickness pin-hole defects.

Coating mechanical, adhesion and wear properties are strongly affected by microstructure. Interfaces with high adhesion are known to ensure prolonged coating life and good wear resistance.[15] Sputtered coating microstructure and physical characteristics depend on the deposition parameters.[15–17] Also, substrate surface conditions prior to deposition, characterized by surface roughness, stress and oxidation state, play an important role in controlling coating properties.[16,17]

In this paper SEM and TEM techniques were used to characterize thicker chromium oxide coating interfacial microstructure as a step towards developing a unique method for depositing thicker coatings with small grains, smooth surface and low residual stress.

*Experimental*

Chromium oxide coatings were deposited on polished low carbon steel substrates by unbiased reactive magnetron sputtering from a 50 mm-diameter Cr target (99.95 % pure) in $Ar/O_2$ plasma (99.99 % pure). The target-substrate separation distance was 60 mm. Deposition was performed at a total pressure of $10^{-1}$ Pa in a mixed Ar and $O_2$ atmosphere with 350 W RF power. Argon flow rate was kept at 20 standard cubic centimeters per minute (sccm), while the oxygen flow rate was 3.2 sccm.

Prior to coating deposition, low carbon steel substrates were cleaned in acetone and ethanol for 10 min in order to remove organic contaminants and then etched for 15 min in an Ar plasma at RF power of 100 W. An 800 nm thick chromium interlayer was sputter deposited for 15 min, after which oxygen gas was introduced into the sputtering chamber for the chromium oxide reactive sputter deposition. The substrate temperature reached 473 K during this 1 hr deposition process, which produced a 4 μm thick coating.

After coating deposition, cross-sections of the specimen were cut, polished and mounted in bakelite for morphological observation. Coating microstructure characterization was performed by scanning electron microscopy (JSM-6301F), and

[*] X. Pang, Dr. K. Gao, Dr. H. Yang, Dr. L. Qiao, Dr. Y. Wang
Department of Materials Physics and Chemistry
University of Science and Technology Beijing
Beijing 100083, China
E-mail: kwgao@mater.ustb.edu.com
Dr. A. A. Volinsky, Dr. X. Pang
Department of Mechanical Engineering
University of South Florida
4202 E. Fowler Ave. ENB 118
Tampa, FL 33620, USA
E-mail: volinsky@eng.usf.edu

transmission electron microscopy (Tecnai F30). Chromium oxide coating cross-section TEM specimens were prepared by ion milling.

*Results and Discussion*

Figure 1 shows SEM cross-section of the chromium oxide coating including the Cr interlayer/substrate interface. The coating is dense with no pores or inclusions present. It survived mechanical polishing, so without any obvious stress concentrators in the coating or at the interface, one can expect good coating adhesion.

Several studies showed that a metal interlayer, 0.5–1.5 μm thick, helps to accommodate coating residual stresses and allows for thicker coatings to be produced, with significant improvements in toughness, adhesion and impact resistance.[18,19]

Sputter-deposited chromium oxide films can have high residual stresses. Coating failures during deposition are primarily due to high residual stress relief. Residual stresses in PVD films and coatings come from two sources: thermal stress and intrinsic (growth) stress. Thermal stresses arise from the mismatch of coating and substrate thermal expansion coefficients. Intrinsic stresses are affected by deposition parameters, specifically by plasma-forming gas pressure, controlled by the forming gas flow rate. Assuming that coating is stress-free at deposition temperature, one can estimate the magnitude of the thermal stress as:

$$\sigma_R^{Thermal} = \frac{\Delta a \Delta T E}{1 - \nu} \qquad (1)$$

where $\Delta a$ is the difference in the coating and the substrate linear thermal expansion coefficients, $\Delta T$ is the difference between deposition and room temperature, $E$ is the coating's elastic modulus, and $\nu$ is the coating's Poisson ratio. The thermal expansion coefficient of chromium oxide ranges from $5.4 \times 10^{-6}$/K to $7.5 \times 10^{-6}$/K, based on its chemical composition. We used $6.5 \times 10^{-6}$/K as a mean value. The steel substrate thermal expansion coefficient is $1.2 \times 10^{-5}$/K. The chromium oxide coating Poisson ratio, $\nu$ is about 0.25, and its elastic modulus is about 230 GPa. Based on these properties

one would estimate 337 MPa compressive residual stress for the chromium oxide coating. This stress level is quite high for ceramic coatings. In order to reduce the amount of thermal stress in the coating, a pure Cr interlayer was deposited prior to the $Cr_2O_3$ reactive sputter deposition.

Intrinsic stresses develop during sputtering and depend on the deposition conditions that control bombarding ions energy and flux.[20] The resulting residual stress is a sum of the intrinsic and thermal stresses:

$$\sigma_R = \sigma_{Intrinsic} + \sigma_{Thermal} \qquad (2)$$

A ductile chromium interlayer aids in coating residual stresses relaxation, and allows the growth of thick coatings without delamination.

Figure 2 shows a TEM cross-section micrograph of the coating, Cr interlayer and the steel substrate. The substrate, interlayer, coating and the interfaces can be clearly seen. A Cr interlayer has columnar grains, whose size increases with the interlayer thickness. There are some defects present in the substrate, and at the steel/Cr interlayer interface, although both the coating and interlayer are dense. Substrate surface defects can act as stress concentration points and affect coating adhesion.

The chromium interlayer has a columnar grain structure (Fig. 2 and Fig. 3(a)). A chromium oxide coating also has columnar grains, but they are much smaller compared to the chromium interlayer, as seen in Figure 3(b). Figure 3(a) shows that there is an amorphous layer present at the interface between the substrate and the Cr interlayer. Figure 3(b) shows an amorphous layer at the interface between the Cr interlayer and the coating. These amorphous layers formed naturally during the deposition process. The formation of amorphous layers may be due to oxygen presence and interfacial lattice mismatch. Even in a fully deposited thin film multilayer systems interfacial reactions involving oxygen are possible, and can be thermodynamically favorable.[21]

There are some benefits to having amorphous layers, as they improve corrosion resistance. There are no grain boundaries, acting as paths of high rate diffusion, leading to prema-
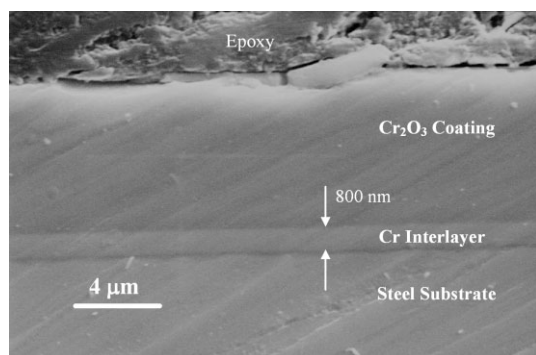


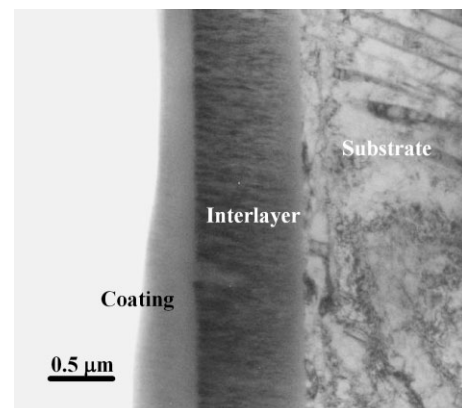*Fig. 1. SEM image of chromium oxide coating cross-section.*
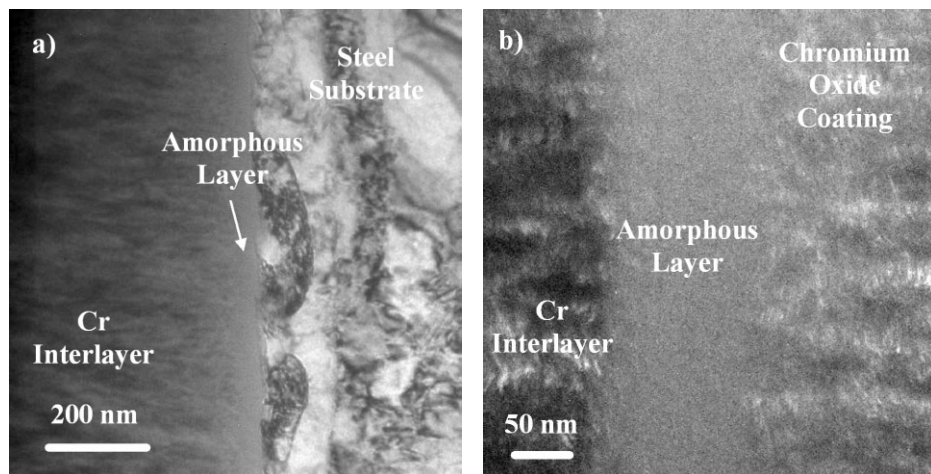


*Fig. 2. TEM micrograph of the coating cross-section.*

Fig. 3. Interfacial microstructure: a) Substrate and interlayer, b) Interlayer and coating.

ture corrosion failures.[22,23] Since most thin films and coatings have a columnar grain structure, grain boundaries would lead the corrosive environment directly to the substrate, compromising corrosion protection. An amorphous layer can also block dislocations motion, thus enhancing the coating strength. Another important amorphous layer function is that of blocking columnar coating grain growth. Coatings with smaller grain sizes are harder, so an amorphous layer present in the middle of the coating thickness would reduce the grain size, which scales with the coating thickness.[24] Larger grain sizes have negative effects on optical and mechanical properties.[25] Figure 4 presents AFM images of 4 and 10 μm thick coatings. Deposition parameters were the same for the two samples of different thickness. The thicker coating has higher surface roughness, 40 nm vs. 5 nm for the thinner coating.

Amorphous layers also allow relieving growth stress in the coating. Chromium oxide coatings are known to have high residual stresses, sometimes exceeding 2 GPa.[2] It is therefore impossible to produce single-layer chromium oxide coatings thicker than 20-25 μm without encountering adhesion problems on typical substrate materials. We have observed thicker coatings to fracture (Fig. 5) due to the high

residual stress relief, as the amount of stored elastic energy per unit area scales with the coating thickness:

$$G = Z \frac{(1 - \nu^2)\sigma_R^2 h}{E} \tag{3}$$

where $Z$ is a constant on the order of unity, Poisson's ratio, $\nu$, $\sigma_R$ is the coating residual stress, $h$ is the coating thickness, and $E$ is its elastic modulus. Thus, thicker coatings are more likely to fracture. The amorphous middle layer approach will reduce the amount of stored elastic energy in the coating by reducing its residual stress, allowing increasing coating total thickness without fracture failures.

The HREM micrograph and diffraction pattern obtained from the middle of Cr interlayer are presented in Figure 6. The Cr interlayer appears to be crystalline. Figure 6(b) shows a diffraction pattern obtained from the Cr interlayer in Figure 6(a). This image reveals a presence of Cr and Fe-Cr intermetallic diffraction rings. Table 1 provides a diffraction ring analysis in terms of the corresponding phase and d-spacing. A precise measurement of the lattice spacing from the HREM image gives inter-planar distances of $d_1 = 0.207$ nm,
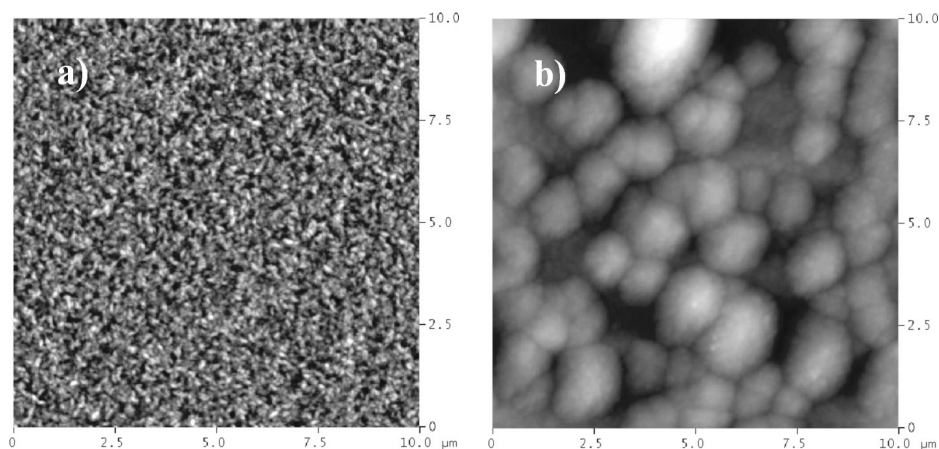


Fig. 4. AFM analysis of coating surface morphology: a) 4 μm thick coating, b) 10 μm thick coating.
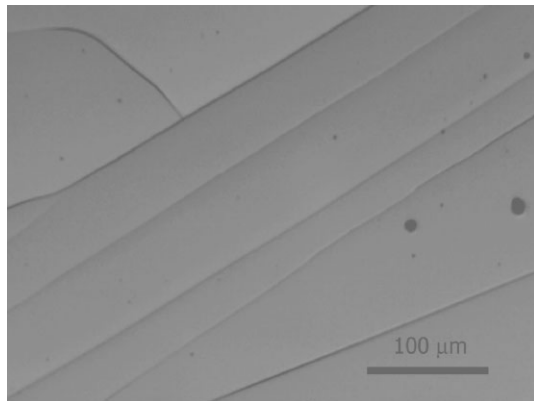
Fig. 5. Optical image of a thicker coating surface fracture. Through-thickness cracks are present in the coating.

Table 1. Experimental and calculated d-spacing values for the diffraction rings of Figure 6(b). [26]

| Ring No. | h k l | d calculated, Å | d experimental, Å |
|---|---|---|---|
| 1 | Cr (110) | 2.04 | 2.07 |
| 2 | Cr (200) | 1.44 | 1.46 |
| 3 | Cr (211) | 1.18 | 1.18 |
| 4 | Fe-Cr (220) | 1.02 | 1.04 |
| 5 | Fe-Cr (310) | 0.909 | 0.909 |
| 6 | Fe-Cr (222) | 0.83 | 0.78 |

$d_2$ = 0.146 nm, $d_3$ = 0.118 nm $d_4$ = 0.104 nm $d_5$ = 0.0909 nm and $d_6$ = 0.078 nm, which is close to Cr(110), Cr(200), Cr(211), Fe-Cr (220), Fe-Cr (310), and Fe-Cr (222), respectively. Measured d-spacing deviation from the theoretical values could be due to the lattice aberration in the interlayer caused by stress. Presence of brittle Fe-Cr intermetallics could affect coating performance. The effect of Fe–Cr phases on the mechanical properties of the coating has to be investigated in more details.

Figure 7 shows high resolution micrographs of the interfaces. There are some defects present on the substrate surface, which act as stress concentrators, so substrate treatment prior to coating depositing is very important for improving coating adhesion strength. While the interfacial layers between the substrate and the Cr, and between the Cr and the coating are amorphous, some nanocrystalline clusters are present in these amorphous layers, as seen in Figure 7(b). A fast Fourier transform and inverse fast Fourier transform analysis of the nanocluster atomic structure showed that these are $Cr_2O_3$ nanocrystals with an atomic spacing of 0.361 nm, which corresponds to the (012) $Cr_2O_3$ inter-planar spacing of 0.363 nm (Fig. 8).

Figure 8 presents HREM and diffraction micrographs of the coating. In Figure 8(a) nanocrystalline grains are sur-rounded by amorphous material. Precise measurement of the lattice spacing from the HREM image gives inter-planar distances of $d_1$ = 0.361 nm and $d_2$ = 0.243 nm. These nanocrystal-line grains are formed of $Cr_2O_3$ due to their similar d-spacing. Actually, the $d_1$ spacing could belong to $d_{012}$ of $Cr_2O_3$, and the $d_2$ to $d_{110}$ of $Cr_2O_3$.[26] In theory, the $Cr_2O_3$ $d_{012}$ distance is 0.363 nm, and $d_{110}$ is 0.247 nm.[26] The measured d-spacing deviation from the theoretical values is due to the residual stress present in the coating. Figure 8(b) is a diffraction pattern obtained from the coating HREM image in Figure 8(a), and shows $Cr_2O_3$ diffraction rings. Table 2 provides diffraction rings analysis. All of the diffraction rings deviate slightly from the standard values for $Cr_2O_3$ in PDF cards due to stress.

Strain in each crystallographic direction of the $Cr_2O_3$ nano-crystals can be calculated as:

$$\varepsilon_{\text{nanocrystals}} = \frac{d_0 - d}{d_0} \qquad (4)$$

where $d$ is the interplanar distance extracted from high reso-lution TEM images and $d_0$ is the unstrained value obtained from a corresponding PDF card.[26] One would calculate enor-
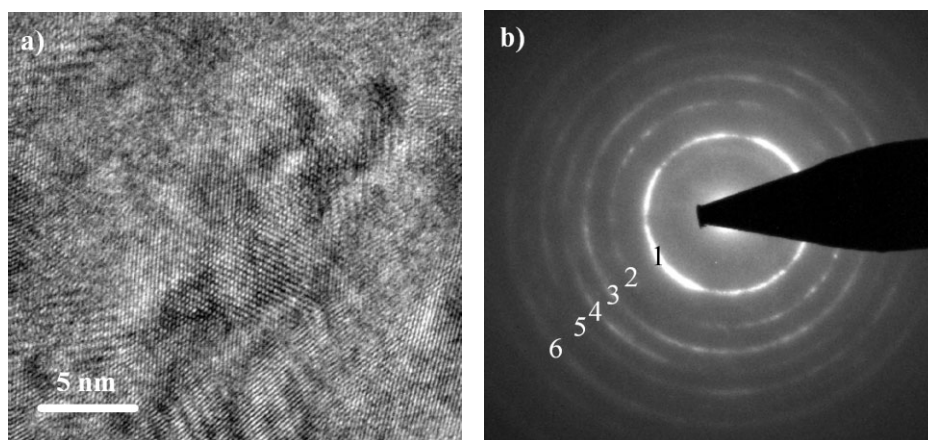


Fig. 6. a) HREM micrograph and b) diffraction pattern of the Cr interlayer.
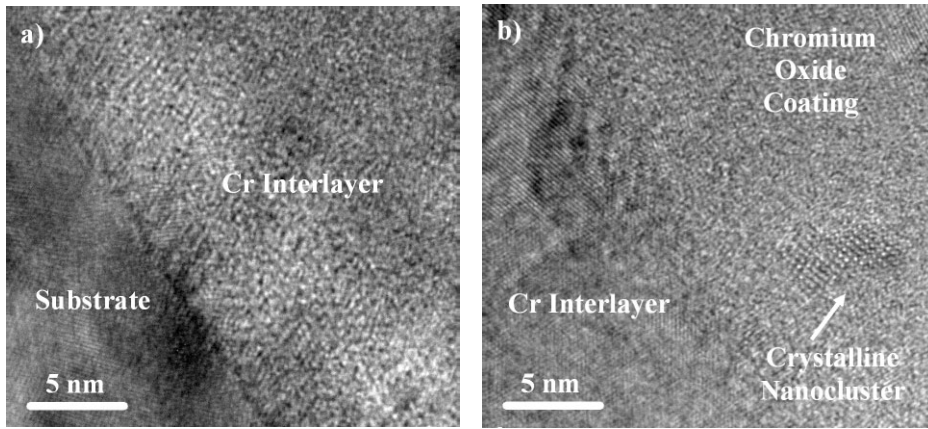
Fig. 7. HREM micrographs of the interfaces between a) the substrate and the Cr interlayer, and between b) the Cr interlayer and the coating.
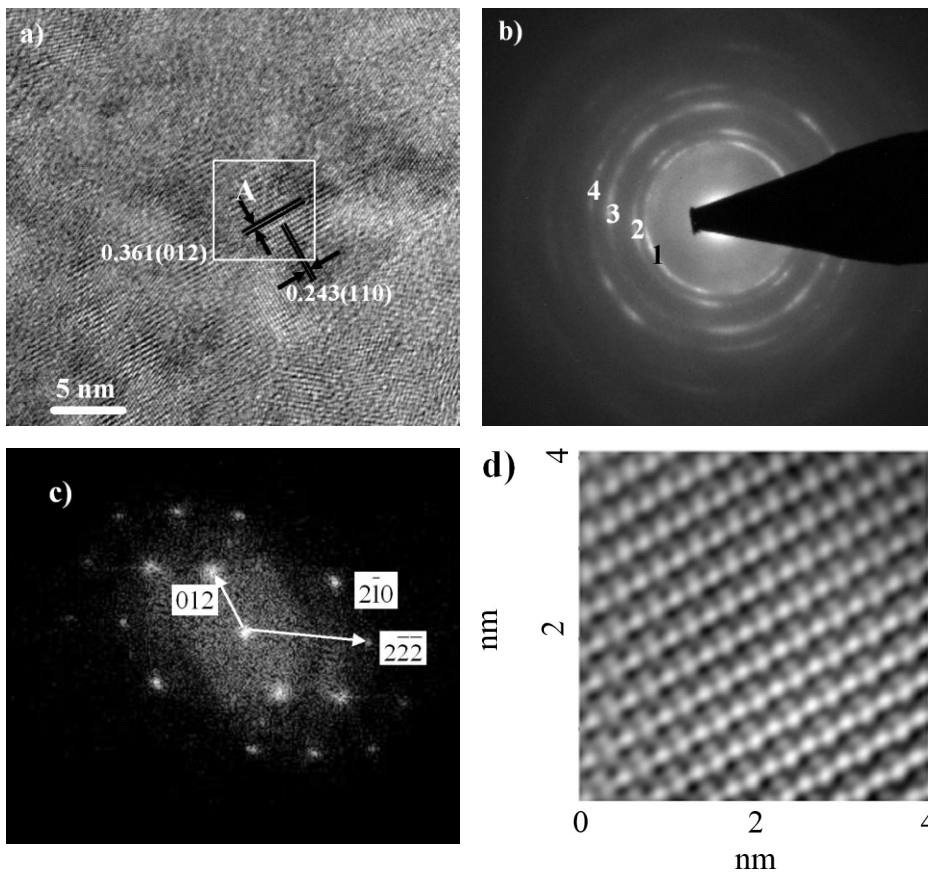


Fig. 8. a) Coating HREM micrograph and b) corresponding diffraction pattern; c) selected area A diffraction pattern; d) image of area A after FFT and inverse FFT.

mous stresses in GPa range by converting the nanocrystalline cluster stain values into stress using appropriate elastic constants and assuming that these nanoparticles are not deformed plastically due to their small size, which prevents dislocation initiation and propagation.[27] The stress in the nanocrystal comes from the volume change associated with the amorphous-to-crystalline transition and the macroscopic residual stress in the coating. Nanocrystals act as stress con-

centrators; however, their percentage in the coating total volume is low except close to interfaces.

*Conclusions*

1. Dense $Cr_2O_3$ coatings were deposited on polished low carbon steel substrates by unbiased reactive magnetron sputtering. There is no obvious porosity and defects in the inter-

*Table 2. Experimental and calculated d-spacing values for the diffraction rings of Figure 8(b).[0]*

| Ring No. | h k l | d calculated, Å | d experimental, Å |
|---|---|---|---|
| 1 | $Cr_2O_3$ (110) | 2.4796 | 2.4836 |
| 2 | $Cr_2O_3$ (113) | 2.1752 | 2.1799 |
| 3 | $Cr_2O_3$ (116) | 1.6723 | 1.6974 |
| 4 | $Cr_2O_3$ (300) | 1.4315 | 1.4394 |

layer and the coating, but the substrate surface defects are present and may affect the adhesion strength.

2. Amorphous layers were detected at each interface, which could block coating columnar grains growth, and allow depositing smooth thick coatings. Amorphous layers also allow relieving growth stress in the coating and depositing thick coatings without any delamination.

3. The deposited Cr interlayer is mainly composed of pure chromium with several Fe–Cr phases detected at the interface between the Cr interlayer and the steel substrate. The presence of Fe-Cr phases may affect adhesion between the substrate and the coating.

4. There are highly stressed $Cr_2O_3$ nanocrystals present in the amorphous layers of the coatings.

[1] U. Rothhaar, H. Oechsner, *Thin Solid Film* **1997**, *302*, 266.

[2] P. Hones, M. Diserens, F. Levy, *Surf. Coat. Technol.* **1999**, *120/121*, 277.

[3] E. Sourty, J. L. Sullivan, M. D. Bijker, *Trib. Int.* **2003**, *36*, 389.

[4] F. D. Lai, C. Y. Huang, C. M. Chang, L. A. Wang, W. C. Cheng, *Microelectronic Eng.* **2003**, *67/68*, 17.

[5] G. V. Samsonov, *in The Oxide Handbook, 2nd edition*, **1982**, 192.

[6] B. Bhushan, G. S. A. M. Theunissen, X. Li, *Thin Solid Films* **1997**, *311*, 67.

[7] B. Bhushan, B.K. Gupta, *Handbook of Tribol. Mater. Coatings and Surf. Treatments*, McGraw-Hill, New York, **1991**, 14.

[8] W. J. Lackey, D. P. Stinton, G. A. Cerny, A. C. Schaffhauser, L. L. Fehrenbacker, *Adv. Ceram. Mater.* **1987**, *2*, 24.

[9] J. Creus, H. Mazille, H. Idrissi, *Surf. Coat. Technol.* **2000**, *130*, 224.

[10] M. Fenker, M. Balzer, H. A. Jehn, H. Kappl, J. J. Lee, K-H. Lee, H-S. Lee, *Surf. Coat. Technol.* **2002**, *150*, 101.

[11] E. Andrade, M. Flores, S. Muhl, N. P. Barradas, G. Murillo, E. P. Zavala, M. F. Rocha, *Nucl. Instrum. Meth. Phys. Res. B* **2004**, *219/220*, 763.

[12] C. Liu, A. Leyland, Q. Bi, A. Matthews, *Surf. Coat. Technol.* **2001**, *141*, 164.

[13] K. D. Bouzakis, S. Hadjiyiannis, G. Skordaris, I. Mirisidis, N. Michailidis, G. Erkens, *Surf. Coat. Technol.* **2004**, *188/189*, 636.

[14] J. H. W. Siu, Lawrence, K. Y. Li, *Wear* **2000**, *237*, 283.

[15] J. D. Olivas, C. Mireles, E. Acosta, E. V. Barrera, *Thin Solid Films* **1997**, *299*, 143.

[16] A. Forn, J. A. Picas, M. J. Simon, *J. Mater. Proc. Tech.* **2003**, *143/144*, 52.

[17] I. Ozdemir, C. Tekmen, S. C. Okumus, E. Celik, *Surf. Coat. Technol.* **2003**, *174/175*, 1064.

[18] A. Leyland, Matthews, *Surf. Coat. Technol.* **1994**, *71*, 19.

[19] G. S. Kim, S. Y. Lee, J. H. Hahn, B. Y. Lee, J. G. Han, J. H. Lee, S. Y. Lee, *Surf. Coat. Technol.* **2003**, *171*, 83.

[20] Y. Pauleau, *Vacuum* **2001**, *61*, 17.

[21] W. Qin, A. A. Volinsky, N. D. Theodore, *Thin Solid Films* **2005**, *473*, 236.

[22] A. Gebert, U. Wolff, A. John, J. Eckert, *Scr. Mater.* **2000**, *43*, 279.

[23] V. Schroeder, C. J. Gilbert, R. O. Ritchie, *Scr. Mater.* **1998**, *38*, 1481.

[24] R. Krishnamurthy, D. J. Srolovitz, *Acta Mater.* **2005**, *53*, 5189.

[25] N. I. Tymiak, A. A. Volinsky, M. D. Kriese, S. A. Downs, W. W. Gerberich, *Metall. and Mater. Trans. A* **2000**, *31A*, 863.

[26] PDF Cards #06-0694, #34-0396, #38-1479PCPDFWIN, Version 2.02, JCPDS-ICDD, **1999**.

[27] W. W. Gerberich, W. M. Mook, C. R. Perrey, C. B. Carter, M. I. Baskes, R. Mukherjee, A. Gidwani, J. Heberlein, P. H. McMurry, S. L. Girshick, *J. Mech. Phys. Solids* **2003**, *51*, 979.